

# ENHANCING CASTABILITY AND FIRE CRACKING RESISTANCE IN 18K ROSE GOLD ALLOYS: CHALLENGES AND SOLUTIONS

Dr. Patrizio Sbornicchia, Dr. Valentina Allodi, Dr. Simone Tomadini, Lorenzo Signorin, Giada Conte, Sofia Casella, Ester Priante, Matteo Giantin, Damiano Zito

> Progold S.p.A. Trissino (VI), Italy

#### **INTRODUCTION**

Among the karat gold alloys, rose and red gold are probably the most susceptible to damage during jewelry manufacturing due to their vulnerability to fire cracking¹ i.e. the appearance of cracks or complete breakage of jewelry as a result of uneven heating. This susceptibility is primarily due to their relatively high copper content, typically ranging between 20%w (42%at) and 25%w (51%at), where ordering phase transformations of the substitutional lattice are highly active, causing dramatic changes in the alloy hardness and reticular parameters upon heating. In fact, the formation of high copper intermetallic (AuCu, Cu 50%at) is reflected in a significant onset of the density curve² during the ordering stage of the alloy (Figure 1).

This implies that the hardening process and thermal expansion act in opposite ways, the former causing contraction and the latter causing expansion, leading to significant mechanical stress in different zones of the jewels. Taking a ring as an example, the zone directly exposed to the flame during firecracking test tends to remain in a hot-annealed state, showing a lower density (Figure 2). The neighbor shanks of the ring can easily experience the appropriate temperature conditions to undergo ordering transformation (zone 1). Once the ordered phase is formed, the increase in density leads to volume restraint of the microstructure, i.e. the individual grains tend to collapse and reduce their volume, potentially leading to fracture due to the high mechanical stress induced (zone 2).

2

ALLODI



Figure 1: Density as function of temperature in 18K red and yellow golds

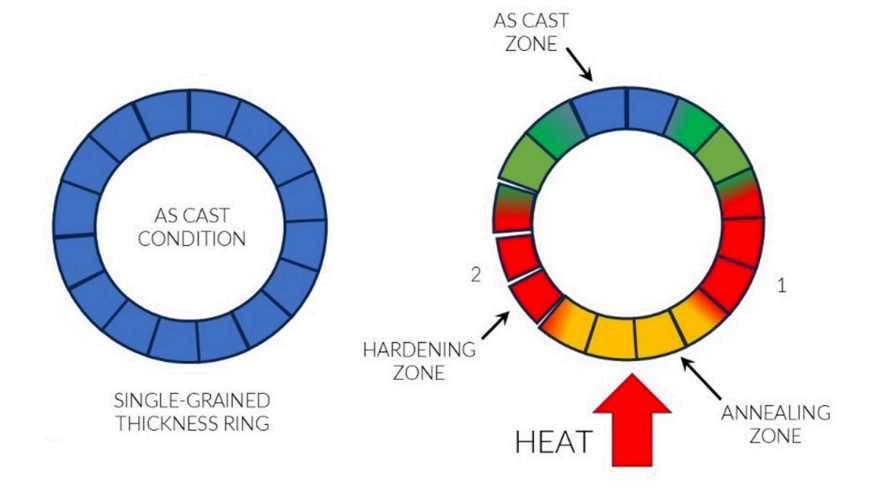


Figure 2: Critical stress zones as function of position into 18K red-gold rings

This doesn't happen with 18K yellow gold, because the lower amount of copper only allow the formation of low copper intermetallic phase (Au<sub>3</sub>Cu), with a smaller change in density

during the ordering process<sup>2</sup> and a decrease in density with temperature that remains essentially linear within the transformation range (Figure 1). The ordered phase, the ascast phase, and the disordered, annealed phase nearly follow the same density variation, and they all lie on the same thermal expansion curve. This means that the hardening process and the thermal expansion follow the same direction and do not provoke contrasting stresses.

The usual approach to increase resistance to firecracking is to add grain refiners such as iridium, ruthenium, rhenium, etc. A grain refiner is generally a high melting chemical element with low solubility in the alloy matrix, whose particles act as seeds to promote faster development of solid phases. In the presence of a grain refiner, solidification occurs at a higher speed because its particles generate a greater concentration of growing crystallites at the same time and their growing boundaries encounter earlier compared to the same alloy without refiner and with fewer nucleation sites.<sup>3</sup>

As a result of this faster solidification, the resulting polycrystalline material will have finer grain size microstructures, which are known to exhibit higher mechanical performances, as evidenced by both an increase in yield strength  $\sigma_v$  (eqn. 8) and in true fracture strength  $\sigma_f$  (eqn. 9) as the grain size (d) becomes smaller.<sup>4,5</sup> The term  $\sigma_0$  in eqn. 8 is called friction stress and is the force required to move a single dislocation in micro-vielded slip band pile-ups confined to isolated grains and corresponds to the resistance of the crystal lattice against the motion of dislocations. The term k<sub>v</sub> is the dislocation locking term and represents the locally intensified stress needed to propagate general yield across the polycrystal grain boundaries. The parameter G and v are the shear modulus and Poisson's ratio of the alloy respectively and V<sub>s</sub> is the free energy of the surface exposed by fracture. The reason why small grain microstructures are stronger and less susceptible to failure than larger grain microstructures are due to the higher number of grain boundaries per unit volume. Grain boundaries are obstacles to single crystal strain, i.e. dislocation movement. As a result, the mechanical strength of the allow is higher, allowing parts to withstand more intense stresses, including the internal stresses induced by sudden density changes.

ALLODI

$$\sigma_y = \sigma_0 + \frac{k_y}{\sqrt{d}}$$
 (eqn. 1)  $\sigma_f = \frac{2G\gamma_s}{\pi(1-\nu)k_y\sqrt{d}}$  (eqn. 2)

However, the application of grain refiners has consistently conflicted with the use of silicon, an essential element in gold alloys for casting purposes since it provides a very clean, deoxidized surface by preventing reactions with the investment material.

In fact, during the investment casting process,  $^{6.7.8}$  several reactions can occur as the molten metal encounters the investment material. These reactions lead to the formation of copper oxides (CuO, Cu<sub>2</sub>O), zinc oxide (ZnO), copper or zinc sulfides (CuS, Cu<sub>2</sub>S, ZnS), and zinc or copper silicates. These reaction products remain on the surface of the tree, causing a loss of brilliance in the as-cast state. Silicon, in combination with zinc, appears to react with oxygen to form a silicate layer that is interposed between the metal and the investment on the outer surface of the metal object. This silicate layer may inhibit the interaction between the molten metal and the investment while also acting as a barrier to prevent the evaporation of metallic zinc from the gold alloy.<sup>9</sup>

A surface free from dark oxides and gypsum residues is particularly crucial for stone-in-place casting, where the pickling process is often more challenging in areas beneath the stones. In these less accessible zones, the alloy may exhibit variations in color and surface finishing. Silicon provides unique brightness, cleanliness, smoothness of castings and affordability, but when its content exceeds a few hundred parts per million, 10,11 it has significant drawbacks, which can be summarized as follows:

- 1. The enlargement of grain size, which reduces the mechanical strength of the alloy.
- 2. The formation of intermetallic compounds, which results in visible hard spots after polishing, due to the silicon strong affinity for refining metals. This not only diminishes the effective deoxidizing and protective role of silicon but may also impair the effect of grain refiners.
- The formation of low-melting or brittle phases with silicon at grain boundaries during alloy solidification, which could compromise the structural integrity of the material (hot tearing effect).

In red gold alloys the first problem is the most critical, while the third problem is less significant due to the higher copper content, which significantly enhances the solubility of silicon within the precious metal matrix.<sup>10</sup> In fact, hot tearing is enhanced by a high amount of gold and silver.

Building on this foundation, our study aimed to find a suitable equilibrium between the silicon content and the amount of refiner. The main approaches explored include the following:

- 1. Varying the amount of grain refiner to minimize its interaction with silicon while assessing whether the refining effect is maintained.
- 2. Testing alternative grain refiners that might offer greater refining effectiveness or less interaction with silicon at equivalent weight proportions.
- 3. Evaluating the refining efficiency based on variations in the particle size of the refining material, keeping its composition constant.

In traditional carat gold, iridium has historically been the most commonly used grain refiner, likely due to its ease of incorporation into copper master alloys and its ability to be optimally homogenized in the final alloy. Its noble character makes it quite resistant to high-temperature oxidation. However, its relatively high solubility in copper means that a higher concentration is required to achieve effective grain refinement, particularly in red karat gold where the copper content is high. This increased concentration greatly elevates both the risk of forming hard spots and the overall alloy cost. An alternative refiner, already well known in the jewelry industry, is ruthenium. The main advantages in using ruthenium are its lower price and the lower content necessary to develop its refining action, due to its very low solubility in copper. However, its extremely low solubility in copper and in the other elements typically found in precious metal alloys has historically made challenging the use of ruthenium as a refiner, particularly due to the difficulty of maintaining a homogeneous concentration. The incorporation of ruthenium into the master alloy to achieve a controlled and homogeneous final concentration has been a technological challenge that has occupied Progold Research & Development and Industrialization departments for remarkable time. The result of this extensive study was the development of a specific method for the incorporation of ruthenium into the master alloy, including both the raw materials used and the production process, as well as the ability to precisely measure ruthenium content. With a reliable method for alloying and a robust analytical system, we were therefore able to thoroughly investigate the effects of ruthenium on 18K red gold alloys throughout this study. In addition to ruthenium, other potential refining additives have been tested, such as molybdenum, tantalum and tungsten, all characterized by high melting temperatures and a minimal to no solubility in gold, with the aim of achieving the smallest possible

size and composition, the free energy of the interface between the refiner and the liquid alloy and the lattice parameter coherence between the refiner and the solid phase. Optimal nucleation site formation occurs when the contact angle approaches zero, meaning the wettability of the liquid alloy on the refiner seeds is nearly maximum.<sup>13</sup>

However, the chemical stability of the refiner is not always consistent over time, and their composition may change during melting and casting processes, especially for finer particles. The smallest particles are likely to dissolve completely, quickly saturating the solvent matrix due to the low solubility of the grain refining elements. In addition, some of these finest particles may completely oxidize due to residual oxygen in the melt and subsequently float to the surface. This oxidation can increase the wetting angle of the molten alloy and thereby reduce their refining effectiveness (Figure 4).

This early process can lead also to a certain ripening of the larger refiner particles, especially if they are already above the critical size described by nucleation theories, 14.15 with the only difference being that in the melting pool the refiner particles are considered as growing nuclei instead of the alloy crystallites themselves. Then it is necessary to consider a possible drift of refiner particles towards a more thermodynamically stable size (Figure 5).

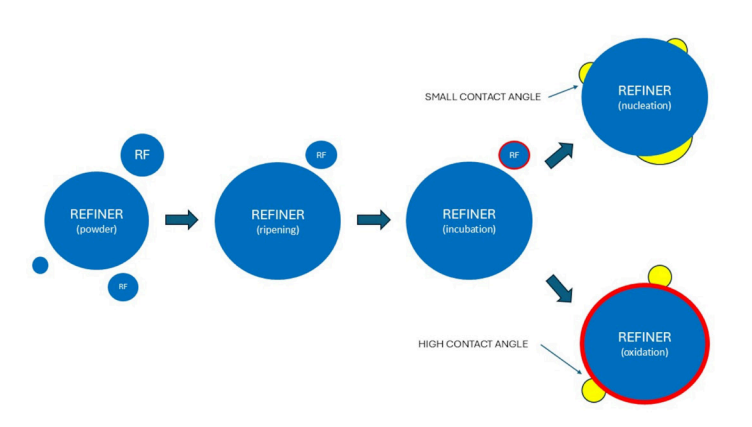


Figure 4: Refiner particles possible evolutions during alloy melting process

grain size and uniform distribution. Also, the role of titanium as a possible grain refiner was explored. This element has a certain solubility in copper and gold at solid state in hot conditions and in this case the refining action may be only due to the formation of refining silicides and oxides.

Another refining approach involved the use of the rare earth element lanthanum, known for its grain-refining capability in steels, commonly attributed to the heterogeneous nucleation of high melting-point lanthanum oxides, oxy-sulfides and sulfides, as well as the segregation of lanthanum in the liquid phase during solidification by *solute effect*.<sup>12</sup>

Finally, the impact on refining performance of maintaining the chemical composition and content of the refiner while utilizing nanometric powders was examined. The nanometric refiners were incorporated into the alloy at the same concentration used in the standard alloying tests. They are expected to promote a significantly greater number of growing crystallites, thereby increasing the resistance of the jewelry to firecracking, since for the same weight content, with smaller particle size, the total number of particles is higher and consequently the number of nucleation sites is enhanced. In the guise of demonstration, the volume occupied by a single 1000  $\mu m$  hypothetically spherical refiner particle  $(5.2 \cdot 10^{-10} \mathrm{m}^3)$  can be fragmented into the overall equal volume of about  $8.0 \cdot 10^{12}$  spherical particles with a diameter of 50 nm. This means that the density of nucleation  $(\eta)$  seeds will be  $8.0 \cdot 10^{12}$  times greater (Figure 3).

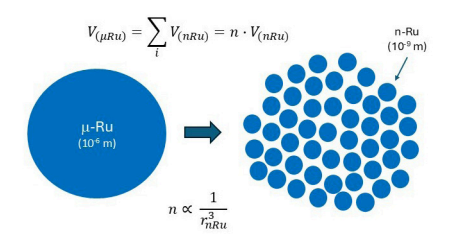


Figure 3: Increase of nucleation density as function of refiner size

Apart from the geometrical aspect, other critical factors must be considered in the context of heterogeneous nucleation of the solid phase. These include the wetting ability of the molten alloy on the refiner particles, the stability of the particles in terms of

8

ALLODI

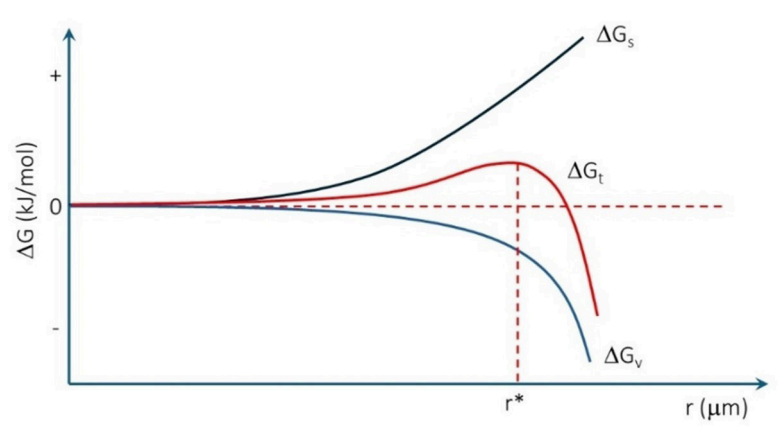


Figure 5: General stability of embryo crystals as function of their size

According to nucleation theories, the stability of solid nuclei, i.e. their total free energy variation ( $\Delta G_t$ ), depends on the balance between the surface energy ( $\gamma$ ) and the volume energy ( $\Delta G_v$ ) contributions (eqn. 10). The crystallites with size smaller than embryos (r\*) or critical size (eqn. 11) tend to dissolve back in molten pool because the surface energy tribute prevails over the volume energy part ( $\Delta G_v$ ) and in the case of grain refiner, they contribute to its saturation in the molten alloy. On the other hand, the crystallites larger than the critical size will grow because the volume contribution to the total free energy dominates over the surface term. The larger crystallites can grow at the expense of the smaller ones that dissolve and saturate the alloy. In the critical size (r\*) equation,  $T_m$  is the melting point of the alloy,  $\Delta H_f$  is its melting enthalpy and  $\Delta T$  is the amount of undercooling during casting.

$$\Delta G_t = \frac{4}{3}\pi r^3 \Delta G_v + 4\pi r^2 \gamma \quad \text{(eqn. 3)} \qquad \qquad r^* = -\frac{2\gamma}{\Delta G_v} = \frac{2\gamma T_m}{\Delta H_f \Delta T} \quad \text{(eqn. 4)}$$

At the steady state of the overheated melt, the refiner particle distribution will be somewhat rearranged and spread throughout its volume, aided by convective motion and electromagnetic stirring. As the melt is poured into undercooled molds, heterogeneous nucleation takes place on the refiner crystallites. Depending on the oxygen scavenging level that can be obtained by argon washing

cycles and deoxidizers, the refiner particles can be coated by more or less thick layers of oxides.

This backside effect could be more visible when smaller amounts of noble refiners were added in atomic form, for instance by means of addition through substitutional prealloy or intermetallic compounds. In this material, grain refiners could be better dispersed in the as fine as possible form into the liquid alloy and greatly increase the nucleation sites but also be oxidized in the fastest way with residual or dissolved oxygen and strongly promote other side reactions, such as carburizing with crucible graphite, intermetallic with formula deoxidizers and salinization. The parasitic synthesis of these refiner compounds could lead to the presence of refiners with different nucleation behavior of the solid phase, making its granular microstructure more inhomogeneous or even giving no refining action at all. It is therefore necessary to find the correct size of the initial refiner added to the composition in order to obtain the smallest grain size and the least oxidation with formation of by-products (Figure 6).

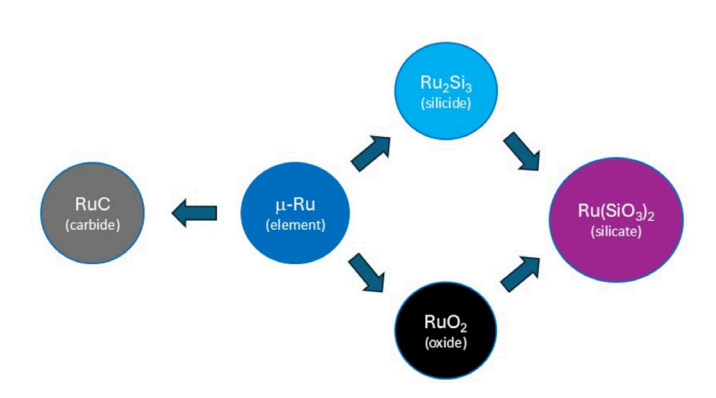


Figure 6: Possible competing pathways with ruthenium as refiner

### **EXPERIMENTAL METHODS**

The alloy compositions used in this research are summarized in Table 1, highlighting the presence or absence of deoxidizers, the type of grain refiners and, for nanometric refiners, their average particle sizes. Alloys m-RG and m-YG serve as reference matrices for red and yellow gold (3N) respectively, with compositions similar to commercial alloys, but without deoxidizer nor grain refiner. These alloys were used to evaluate the fire cracking resistance of the base alloys, underlying the differing behavior of red and yellow gold matrices and providing a baseline for assessing

ALLODI

13

the subsequent effects of refiners and deoxidizers.

The alloys r-RG and r-YG have the same basic composition of red or yellow matrix alloys, but with the addition of iridium as traditional grain refiners in order to study its effect on the behavior of carat gold. The effect of the contemporary presence of silicon and refiners is evaluated starting from alloy (A). The difference between alloy (A) and (B) lies in the iridium content, which is higher in the former and lower in the latter, while alloy (C) has ruthenium as a refiner, introduced following Progold's standard procedure. The alloys with alternative refiners start from (D) to (H). Ruthenium was introduced as a nanometric powder starting with alloy (I), with a decreasing average size starting with alloy (I), alloy (M), and finally alloy (N). The last alloy (O) is made with probably the finest form of ruthenium, using an intermetallic compound ( $Ru_xM_y$ ) that should release the element in very small embryos, undissociated molecules or even atoms.

Table 1: Alloy compositions

ALLOY	Au (%w)	Cu (%w)	Ag (%w)	Zn (%w)	Si	lr	Ru	Ta	w	Мо	La	Ti
m-RG	75.2	23.0	1.0	0.7	no	no	no	no	no	no	no	no
m-YG	75.2	15.0	15.0	0.7	no	no	no	no	no	no	no	no
r-RG	75.2	23.0	1.0	0.7	no	yes	no	no	no	no	no	no
r-YG	75.2	15.0	15.0	0.7	no	yes	no	no	no	no	no	no
Α	75.2	23.0	1.0	0.7	yes	yes↑	no	no	no	no	no	no
В	75.2	23.0	1.0	0.7	yes	yes↓	no	no	no	no	no	no
С	75.2	23.0	1.0	0.7	yes	no	yes	no	no	no	no	no
D	75.2	23.0	1.0	0.7	yes	no	no	no	yes	no	no	no
Е	75.2	23.0	1.0	0.7	yes	no	no	yes	no	no	no	no
F	75.2	23.0	1.0	0.7	yes	no	no	no	no	no	yes	no
G	75.2	23.0	1.0	0.7	yes	no	no	no	no	yes	no	no
Н	75.2	23.0	1.0	0.7	yes	no	no	no	no	no	no	yes
ı	75.2	23.0	1.0	0.7	yes	no	nano size 1	no	no	no	no	no
L	75.2	23.0	1.0	0.7	yes	no	nano size 2	no	no	no	no	no
М	75.2	23.0	1.0	0.7	yes	no	nano size 3	no	no	no	no	no
N	75.2	23.0	1.0	0.7	yes	no	nano size 4	no	no	no	no	no
0	75.2	23	1.0	0.7	yes	no	Ru <sub>x</sub> M <sub>y</sub>	no	no	no	no	no

For alloys refined with alternative elements or ruthenium in nonstandard forms, the refiner concentration was kept as constant as possible and equal to the concentration typically used for ruthenium-refined alloys, such as alloy (C), to have a direct ponderal comparison of the refining effect.

The preparation of each gold alloy started with the production of a master alloy. The master alloys containing iridium, ruthenium, lanthanum or titanium as grain refiners were cast in a closed melting machine with a controlled atmosphere equipped with a granulating unit (Indutherm, VC480 V). Inert gas was employed to protect the melting pool, and the material was heated and homogenized at 1200°C (2192°F) before being poured into water.

The addition of tungsten, molybdenum and tantalum to the master alloy was tested using different operating methods and different raw material formats, including nanopowders. For tungsten and molybdenum, the best results were obtained by melting in a closed tilt-casting machine (Galloni Pressovac Max XL) under inert gas at temperatures ranging between 2000-2100°C (3632-3812°F), using non-nanometric elements. In this case, the material was not granulated in water but poured into an ingot mold. The resulting prealloys were then combined with other elements to obtain the master alloy into the previously described granulating casting machine. The actual concentration of the refiner in the master alloys was verified by inductively coupled plasma optical emission spectrometry (ICP-OES Perkin Elmer Avio 220 Max). wavelength dispersive X-ray fluorescence spectrometry (WD-XRF Bruker, Tiger S8) or spark optical emission spectrometry (SPARK-OES), depending on the analyzed element. This verification was necessary because some properties of the elements used as refiners, such as high melting point and tendency to oxidize, can result in a lower concentration in the master alloy than intended. This occurs, for example, because a higher percentage of these elements accumulates in the melt residues, either as decanted or floating material. The qualitative results of these analyses are shown in Table 2. In the cases with compositions where multiple melt tests were performed, the table shows the result from the test with the concentration closest to the intended value.

Table 2: Verification of refiners in master alloys and used instrumental techniques

MASTERALLOY	REFINER	QUANTITY DETECTED	TECHNIQUE
A	HIGH IRIDIUM	AS INTENDED	WD-XRF SPARK-OES
В	LOWIRIDIUM	AS INTENDED	ICP
С	STANDARD RU	AS INTENDED	WD-XRF
D	TUNGSTEN	LOWER	ICP
E	TANTALUM	NOT DETECTED	ICP
F	LANTHANUM	LOWER	ICP
G	MOLYBDENUM	LOWER	ICP
Н	TITANIUM	AS INTENDED	WD-XRF
1	NANO RU SIZE 1	AS INTENDED	WD-XRF
L	NANO RU SIZE 2	AS INTENDED	WD-XRF
М	NANO RU SIZE 3	AS INTENDED	WD-XRF
N	NANO RU SIZE 4	AS INTENDED	WD-XRF
0	RU INTERMETALLIC	AS INTENDED	WD-XRF

In certain cases, such as molybdenum, tungsten and lanthanum, even the best melting test performed to date yielded results below the theoretical target. Nevertheless, it was decided to proceed with the firecracking tests because the amount of refiner detected could still have a noticeable effect. In addition, for some of these elements, it is likely that the maximum solubility limit in the matrix had effectively been reached. The only unacceptable case was tantalum, which by all accounts never seemed to enter the copper matrix even in trace amounts. In this case, it was decided not to proceed with alloying with gold and fire cracking tests.

ALLODI

The gold alloys were prepared by the same granulating process described for the master alloys, but at a lower temperature (1050°C\1955°F). The subsequent investment casting was then performed at a casting temperature of 1000°C\1832°F and 650°C\1202°F for the flask. After casting, the flasks were allowed to cool for five minutes under casting pressure, i.e. 1.5 bar overpressure from the crucible chamber and -1.0 bar suction from the flask side and then cooled in water. Each casting tree was photographed before and after pickling to document surface oxidation and investment residue. The investment casting process was repeated multiple times to improve the statistical reliability of the results.

The cast objects were designed to exhibit different types and degrees of mechanical stress under uneven heating conditions, while also representing different types of jewelry (Figure 7). For

example, the bridge rings (1) have two subtle joints on the head and thickness variation on the shanks to evaluate the resistance of the alloys with uneven shapes. The heavy wedding rings (2) were introduced to check the resistance of the alloy under mechanical stress due to round closed shape items. The heavy open earring (3) was used for the same reason, but in round open items also subjected to a bending load. The butterfly filigree items (4) were used to evaluate the mechanical resistance of the thin thickness under local thermal treatment. Simple rectangular and thick medals (5) were also cast for analysis of hard spots, grain size, and color measurements.

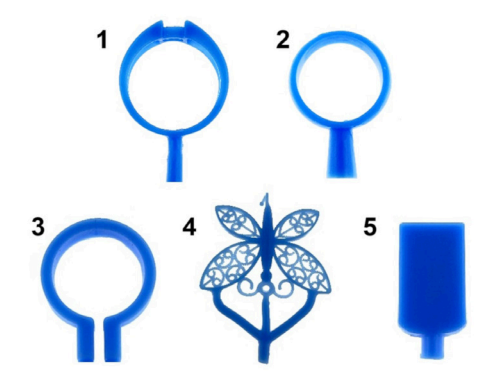


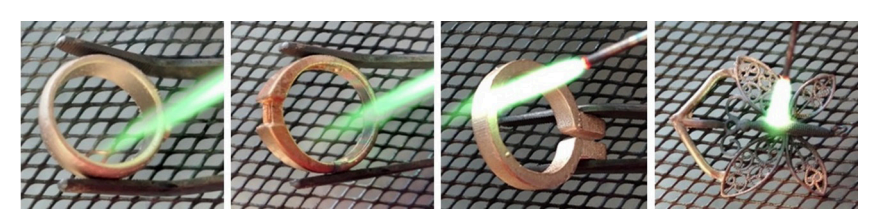
Figure 7: Cast items



Figure 8: Tree architecture

The cast tree was mounted according to an architectural order of five levels (Figure 8) each level having three items, the top one constituted by items (4), the second one of medals (5), the third one of bridge rings (1), the fourth one of wedding rings (2) and the last one close to the tree bullion made of earrings (3).

The parts were removed from the main sprue and individually tested for resistance to fire cracking. This test consisted of localized heating of the parts by flame from the combustion of a mixture of oxygen and hydrogen produced by the electrolysis of alkaline water, commonly referred to as water soldering. The heating on a small area of the items induces a differential thermal treatment in a completely analogous manner to soldering process in jewelry, which also provides a different degree of age hardening as a function of the distance from the flame. Each piece was flamed for two minutes, always insisting on the same small zone (Figure 9). The differential hardening gives high stress zones causing more or less serious fractures.



ALLODI

Figure 9: Firecracking test



Figure 10: Microcrack example



Figure 11: Crack example

Firecracking resistance was evaluated based on the number of cracks and microcracks found under optical observation at typical goldsmithing magnification (10-20x) using a stereomicroscope (Nikon, SMZ800). In this study, a microcrack was conventionally classified as a separation between two grains without evidence of crack enlargement, i.e. the gap between the grains remains very thin (0-20  $\mu$ m) and approximately constant (Figure 10). On the other hand, a crack has been conventionally defined as a more or less long gap between grains with clear evidence of enlargement, for example from 20 to 100  $\mu$ m (Figure 11). For practical purposes, cracks are easily visible to the naked eye, while microcracks are mainly visible under a microscope.

Medal samples were polished on both sides on a lapping machine with 1 µm polycrystalline diamond suspension on a cloth disk as the last stage (Buehler, ECOMET) and then examined by means of a stereozoom optical microscope for the presence of hard spots up to 50X magnification. For potential and suspected hard spots, their composition was confirmed by microanalysis in a scanning electron microscope (ZEISS, Evo10 SEM-EDX).

The polished medals were also subjected to metallographic analysis using dilute potassium cyanide solution and few drops of hydrogen peroxide (H2O2) as accelerating and coloring agents. The resulting microstructure was measured using a digital microscope (KEYENCE, VHX5000) equipped with a plug-in for grain counting and sizing.

19

## **RESULTS AND DISCUSSION**

The reference alloys in karat gold (m-RG, m-YG) clearly show the absence of any additives, such as deoxidizers and refiners, being their trees the most oxidized in the as-cast conditions (Figure 12, Figure 13). After pickling in fluoboric acid (HBF $_4$ , H $_2$ O $_2$ ), the dark oxides can be easily removed, but the surface composition is stripped of the less noble elements (Cu, Zn), resulting in a color shift and especially in stone-in-place or filigree castings, the original alloy color cannot be adequately restored (Table 3).



Figure 12: Appearance of reference red gold 18K (m-RG) before and after pickling



Figure 13: Appearance of reference yellow gold 18K (m-YG) before and after pickling.

With the simple addition of a grain refiner (r-RG), the tree still appears dark and opaque in the as-cast condition, though less severely, with gypsum-contaminated surfaces (Figure 14). The aspect remains opaque even after pickling. With the addition of silicon to the composition, the appearance of the cast tree is shiny and bright, as shown in Figure 15 for alloy (A). All of the siliconcontaining compositions examined in this study exhibit this as-cast appearance and their color is quite close to the target of standard red gold alloy, namely alloy r-RG (Table 3).



Figure 14: Appearance of refined red gold 18K (r-RG) before and after pickling.



Figure 15: Appearance of red gold 18K with silicon (A) before and after pickling.

Table 3: Cast alloys color coordinates (CIELab)

ALLOY	L*	A*	B*	ΔE <sub>00</sub>
m-RG	86.03	8.89	16.98	0.46
m-YG	89.68	3.06	22.69	7.72
r-RG	86.73	8.80	16.83	TARGET
r-YG	88.88	3.46	24.23	7.60
Α	86.46	8.53	16.62	0.25
В	85.81	8.78	17.29	0.65
С	86.33	8.55	16.88	0.36
D	85.72	8.79	17.14	0.68
E	-	-	-	-
F	86.48	8.50	16.71	0.32
G	85.44	8.76	17.02	0.85
Н	85.45	8.88	17.08	0.85
I	86.26	8.53	16.6	0.35
L	85.95	8.69	17.16	0.57
М	86.61	8.45	16.68	0.28
N	86.59	8.47	16.76	0.30
0	85.58	8.76	17.09	0.77

The grain sizes measured by digital microscopy (Keyence, VHX) on both sides of the medals after cyanide etching are reported in Table 4, along with the number of hard spots.

Grain dimensions could vary depending on the side of the medal because the distribution of grain refiner during solidification could be uneven. In fact, the density of the grain refiner can affect its distribution depending on whether it is lighter or denser than the molten alloy. A refiner with a much lower density than the host matrix tends to float on the molten pool, while a refiner with a much higher density will tend to precipitate at the bottom of the crucible. This tendency can also be appreciated on the upper and lower faces of the flat medallion used in this study, where it is intended for the upper face the one that is towards the tree apex and for the lower face the one that is down looking at the tree

bullion. Computer simulations of the solidification process for the thick medal, performed using ProCAST (ESI) software, indicated that the time required for the item to completely fill and reach the solidus temperature was approximately two to three minutes. This time could be long enough to enable a refiner repartition between the upper and lower face of the medal, thus showing a differential grain refinement. In the case of iridium, the difference between its density (22.56 g/cm<sup>3</sup>) and the density of the molten gold alloy (13.60 g/cm<sup>3</sup>) is very high, consequently it is much more probable for the upward medal face to display a remarkable smaller grain size. In fact, alloys (r-RG) and (r-YG) have an upper surface grain size three and four times smaller than the corresponding lower surfaces. On the other hand, the density of ruthenium (12.36 g/ cm<sup>3</sup>) is lower than that of iridium and quite similar to that of the molten matrix. The difference in grain size between the top and bottom surfaces in this case reaches a maximum of twice the size, indicating that ruthenium tends to promote a more uniform grain distribution throughout the bulk of the item.

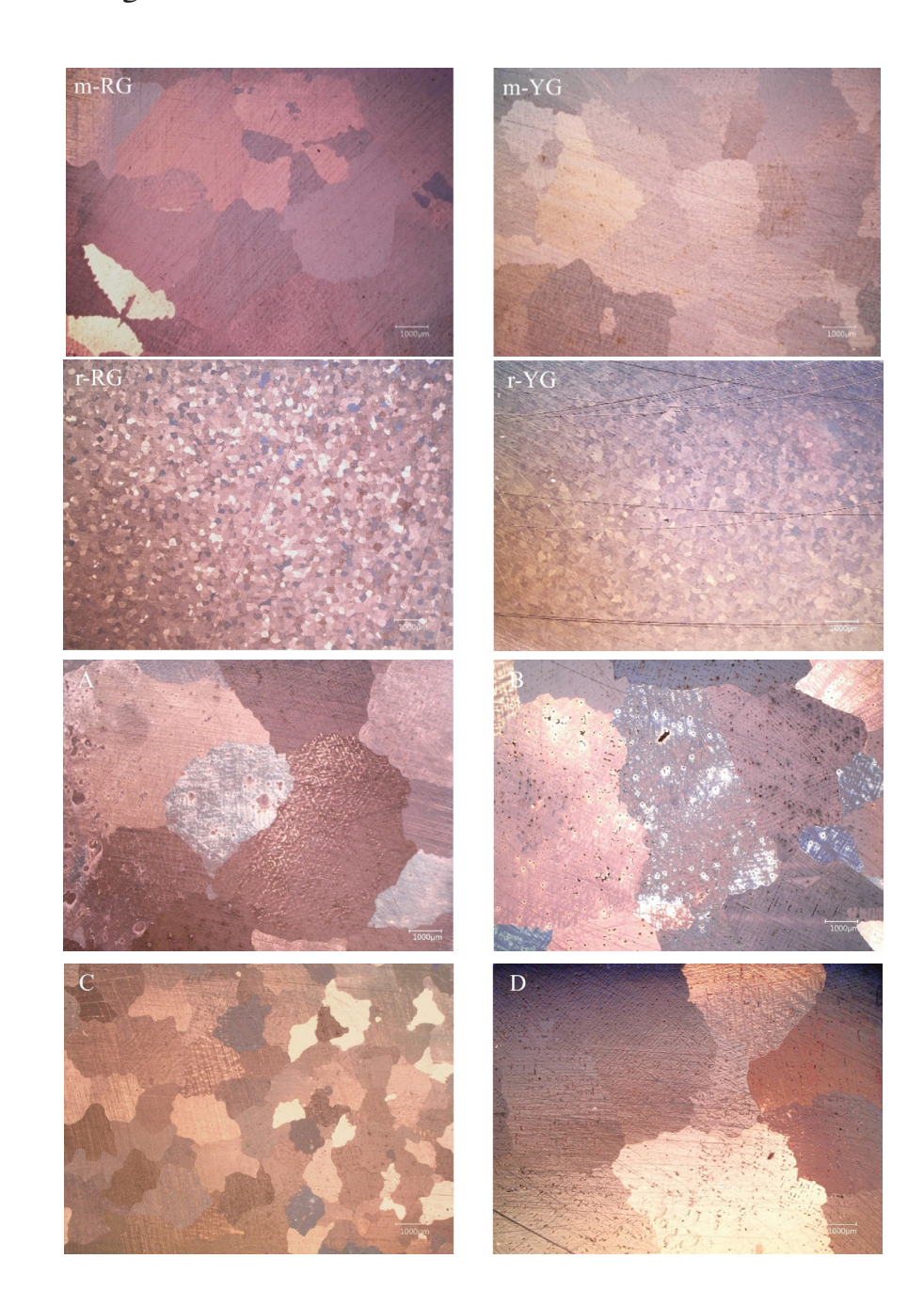
If we look at the grain size of the different alloys (Figure 16 and Figure 17), we can see the extreme reduction in size from the simple matrix alloys (m-RG and m-YG) to the iridium-refined alloys (r-RG, r-YG). The addition of silicon causes an almost 10-fold increase in grain size (alloys A and B), from an average value of 250  $\mu m$  to almost 3000  $\mu m$ . By simply switching the refiner from iridium to standard ruthenium (alloy C), the average grain size is reduced to approximately 1200  $\mu m$ . The transition to nanometric refining particles further decreases the average grain size by nearly 40% (Figure 18). In contrast, the use of ruthenium intermetallic compounds proves to be less effective in achieving significant grain refinement.

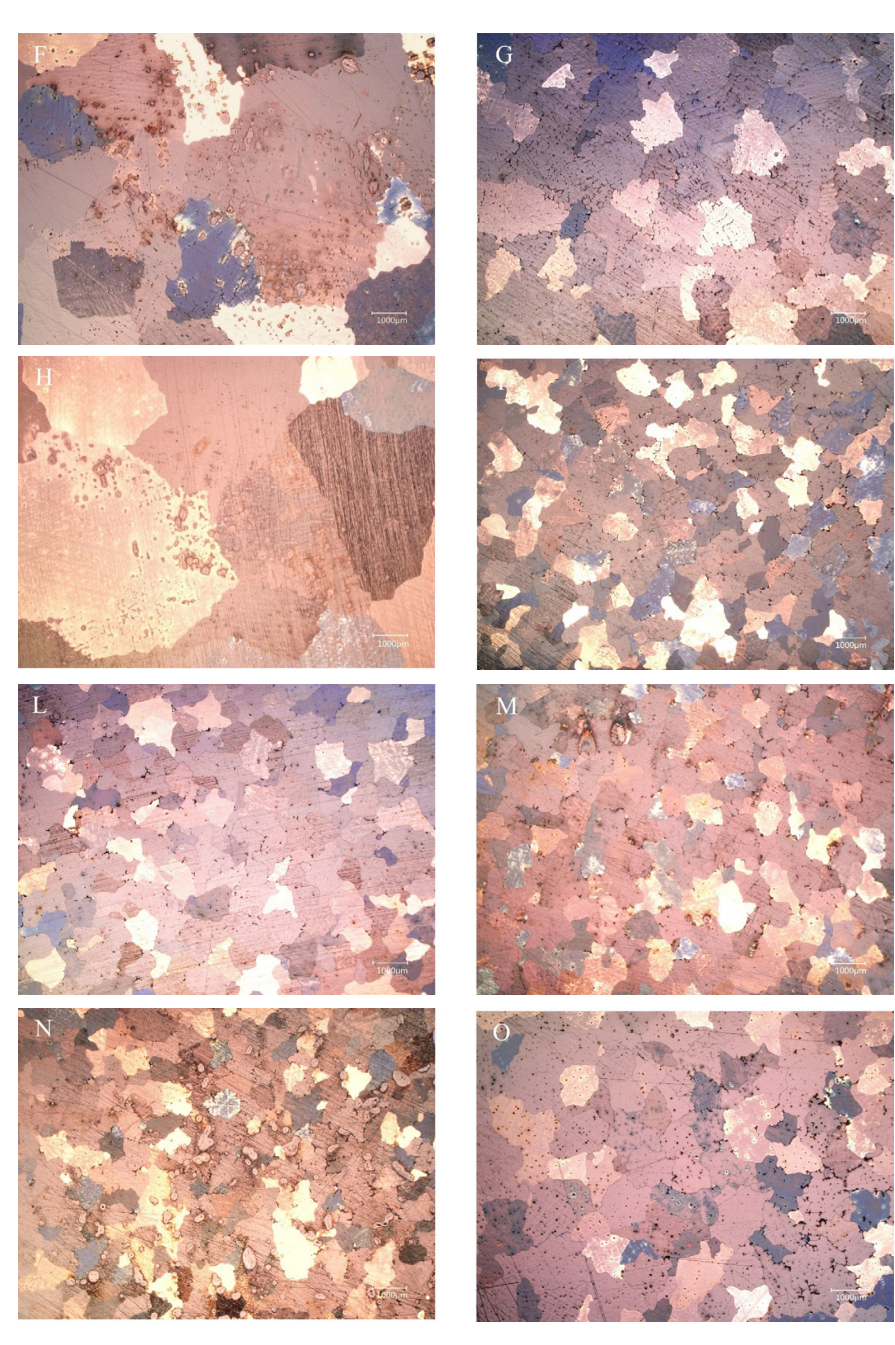
Of the other elements tested, tungsten (alloy D) and titanium (alloy H) do not show a reduction in average grain size compared to alloys A and B. Conversely, lanthanum (alloy F) appears to have a mild refining effect, while molybdenum (alloy G) proves to be as effective as standard ruthenium in refining grains. The tantalum alloy (E) is missing from the list because of the lack of refiner in the master alloy.

	HARD	GRAII	N SIZE	
ALLOY	SPOTS	UP (µm)	DOWN (µm)	
m-RD	0	1855 ± 829	1672 ± 786	
m-YG	0	2103 ± 890	2000 ± 829	
r-RG	0	136 ± 52	397 ± 184	
r-YG	0	167 ± 67	706 ± 325	
A	0	3239 ± 1321	2448 ± 1280	
В	0	3833 ± 1503	3599 ± 2270	
С	0	955 ± 387	1405 ± 851	
D	0	3192 ± 1596	2739 ± 1394	
F	0	1910 ± 1084	1906 ± 1012	
G	0	920 ± 456	1277 ± 878	
н	0	2822 ± 1649	4252 ± 1436	
ı	0	646 ± 296	1157 ± 668	
L	0	738 ± 302	1059 ± 568	
М	0	743 ± 285	1093 ± 601	
N	0	626 ± 272	1038 ± 547	
0	0	1021 ± 348	1566 ± 772	

ALLODI

Figure 16 (series of photos on this page and the next) shows the appearance and grain size of the studied alloys after metallographic etching.





ALLODI

Figure 16: Alloy grains after metallographic etching

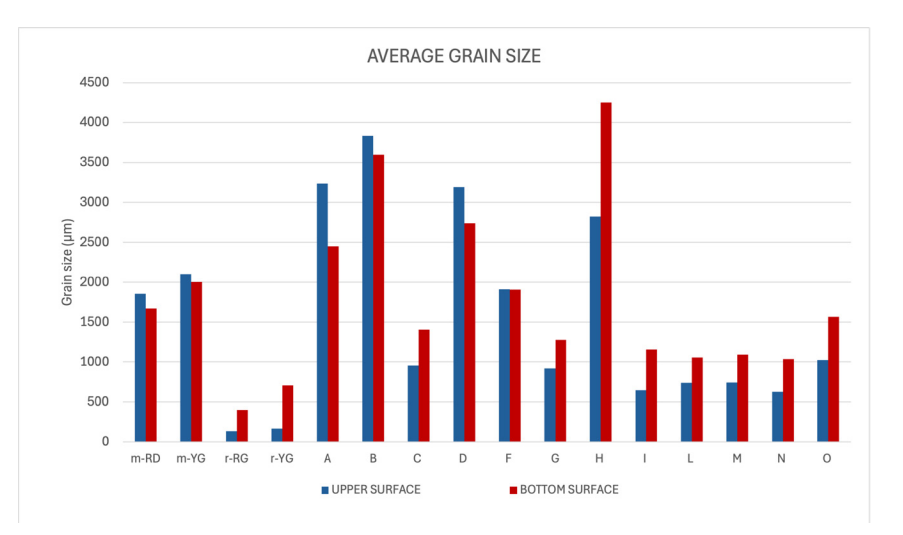


Figure 17: Alloys average grain size

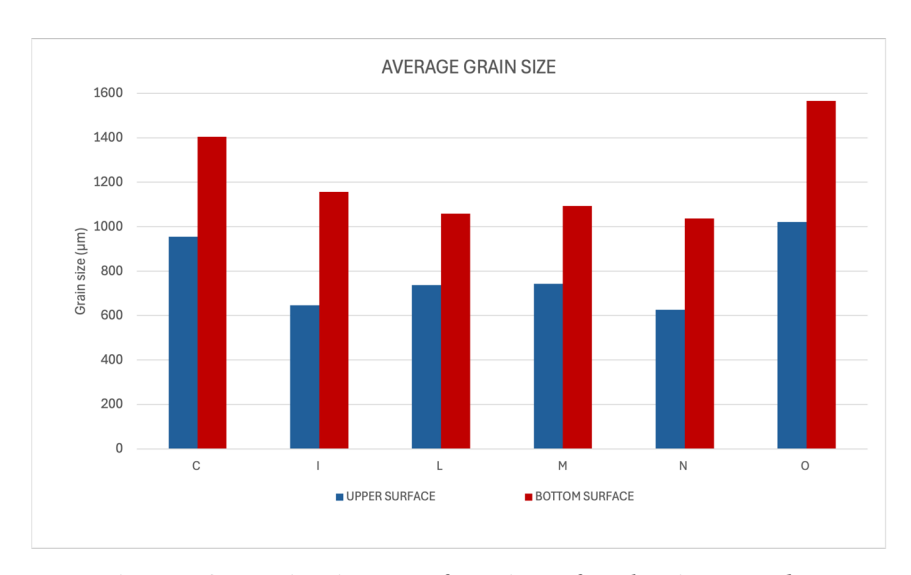
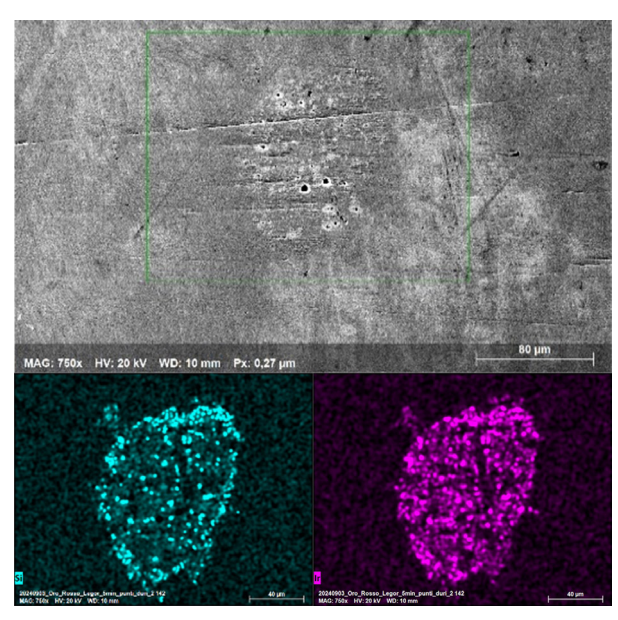


Figure 18: Grain size as a function of ruthenium used, from standard Ru (C) to size 1 nano-Ru (I), size 2 nano-Ru (L), size 3 nano-Ru (M), size 4 nano-Ru (N) and intermetallic Ru (O)

Figure 19 illustrates how silicon can subtract the grain refiner by forming insoluble precipitates in a commercial alloy with iridium and silicon. Precipitates detection is quite challenging, even using backscattering mode during scanning electron microscopy analysis (SEM-BS), as they are hardly distinguishable from the host matrix.

The precise stoichiometry of these intermetallic compounds is not clear, but it is reasonable to suppose they are a form of iridium silicide. Thereby, silicon becomes a refiner scavenger subtracting iridium from precious matrix and reducing its capacity of reducing the grain size. Although in some lucky cases, small intermetallic particles could act as grain refiners, when they start to collapse into larger clouds like into these alloys their refining action is hindered.

Ruthenium can also react with silicon, but due to its much lower solubility in the copper master alloy and the limited amount added to the composition, ruthenium silicides are less probable to appear as hard spots after polishing. Notably, no hard spots were observed in any of the tested alloys, indicating that the refiner content is well-balanced in the final alloys.



ALLODI

Figure 19: Typical hard-spot morphology and composition in a commercial alloy with iridium and silicon

Table 5 summarizes the incidence of cracks and microcracks for the different alloys. The data are presented as the average number of cracks and microcracks per specimen (n, N) and the percentage of fractured specimens relative to the total number of specimens analyzed (n%, N%). Completely fractured items are referred to as "crash" specimens (Figure 20).





Figure 20: Typical crash in wedding and bridge rings

Table 5: Overall cracks and microcracks detected

ALLOY	BRIDGE	BRIDGE RINGS WEDDING		RINGS EARR		INGS	BUTTERFLIES	
ALLOY	MICROCRACKS	CRACKS	MICROCRACKS	CRACKS	MICROCRACKS	CRACKS	MICROCRACKS	CRACK
	(n, n+)	(N, N+)	(n, ns.)	(N, N <sub>h</sub> )	(n, n+)	(N, N <sub>11</sub> )	(n, ns)	(N, N <sub>h</sub> )
m-RG	4.0	0.3	0.0	0.0	15.0	8.0	0.7	0.3
	67%	33%	0%	0%	100%	100%	67%	33%
m-YG	0.0	0.0	0.0	0.0	0.0	0.0	0.0	0.0
	0%	0%	0%	0%	0%	0%	0%	0%
r-RG	0.0	0.0	0.0	0.0	0.0	0.0	0.0	0.0
	0%	0%	0%	0%	0%	0%	0%	0%
r-YG	0.0	0.0	0.0	0.0	0.0	0.0	0.0	0.0
	0%	0%	0%	0%	0%	0%	0%	0%
Α	crash	crash	crash	crash	crash	crash	crash	crash
В	crash	crash	crash	crash	crash	crash	crash	crash
С	2.9	1.0	5.0	1.1	1.8	0.3	0.7	0.1
	89%	33%	89%	44%	22%	11%	33%	11%
D	crash	crash	crash	crash	crash	crash	crash	crash
F	crash	crash	crash	crash	crash	crash	crash	crash
G	crash	crash	8.0 100%	3.0 100%	13.0 100%	10.0 100%	1.0 67%	5.0 67%
н	crash	crash	9.0 100%	3.0 100%	crash	crash	crash	crash
ı	3.0	2.3	2.0	0.7	0.5	0.3	0.2	0.2
	50%	50%	67%	33%	17%	17%	17%	17%
L	0.9	1.4	2.0	0.1	0.0	0.0	0.2	0.0
	11%	22%	44%	11%	0%	0%	11%	0%
М	0.7	0.2	0.8	0.0	0.5	0.0	0.0	0.0
	33%	17%	67%	0%	33%	0%	0%	0%
N	1.2	0.0	1.2	0.2	0.5	0.0	0.0	0.0
	33%	0%	67%	17%	33%	0%	0%	0%
o	2.0 67%	0.7 33%	2.3 67%	0.7 67%	4.7 33%	0.3 33%	0.0	0.0

In general, the rule that a reduction in grain size leads to a reduction in the number of cracks and an increase in fracture toughness is largely confirmed, although there are some exceptions. The smallest grains in the iridium-refined traditional red and yellow alloys (r-RG, r-YG) result in perfect firecracking resistance. In the reference matrix alloys (m-RG, m-YG), despite the large grain size in both cases, only m-RG shows significant failure sensitivity due to its pronounced heterogeneous age hardening.

The most notable exception to this trend is the molybdenum-refined alloys (G), which, despite having a grain size very similar to that of standard ruthenium-refined red gold (C), resulted in almost completely fractured specimens when firecracked. A possible factor contributing to this brittle failure could be the accelerated formation of oxides at grain boundaries, possibly influenced by the presence of certain elements. This aspect needs to be investigated in future research.

The fracture incidences (n, N) for each items and the fraction of fractured items on the total  $(n_{\%}, N_{\%})$  are reported in graphical form to give a detailed vision and better comprehension of this general trend (Figure 21-Figure 28).

ALLODI

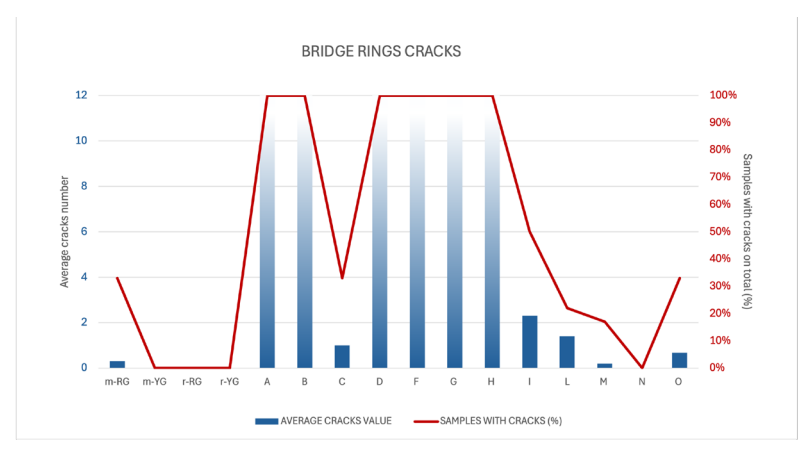


Figure 21: Average cracks per items and cracked items percent for bridge rings

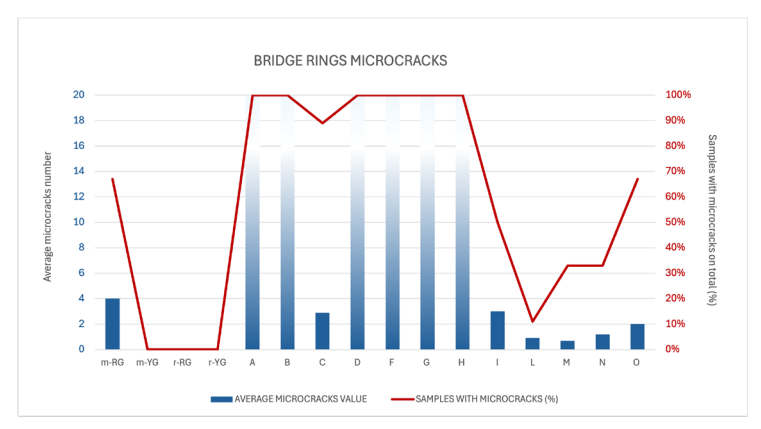


Figure 22: Average microcracks per items and microcracked items percent for bridge rings

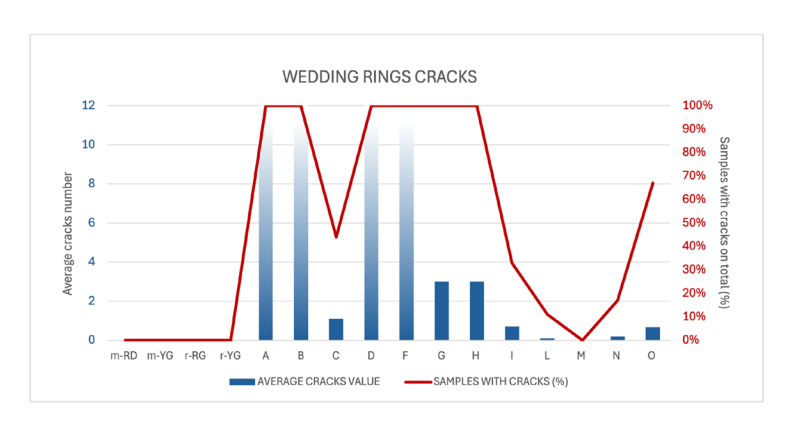


Figure 23: Average cracks per items and cracked items percent for wedding rings

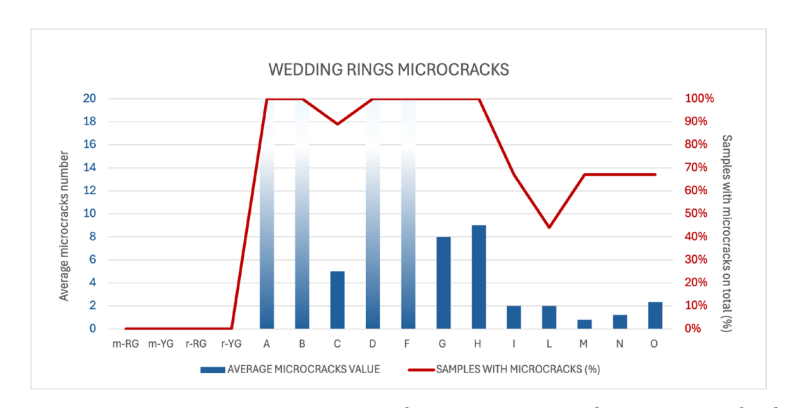


Figure 24: Average microcracks per item and microcracked items percent for wedding rings



Figure 25: Average cracks per item and cracked items percent for earrings



ALLODI

Figure 26: Average microcracks per items and microcracked items percent for earrings

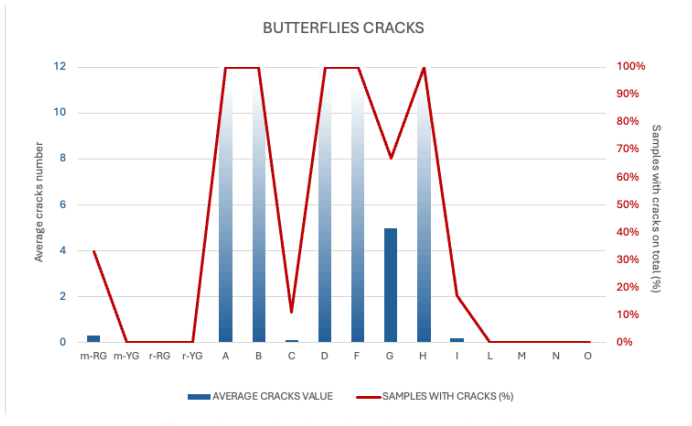


Figure 27: Average cracks per item and cracked items percent for butterflies

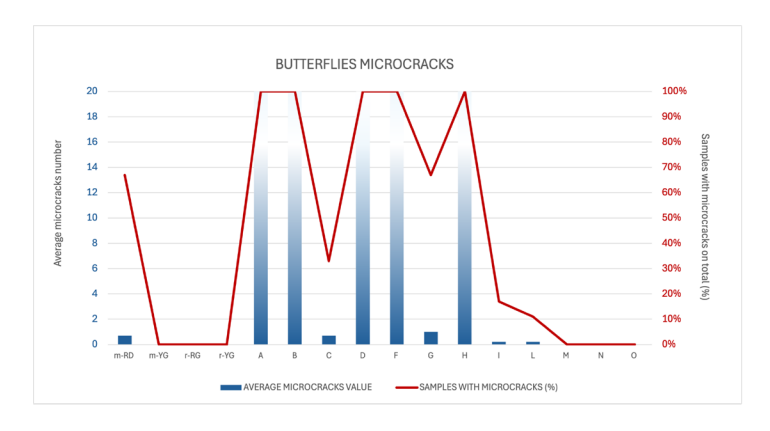


Figure 28: Average microcracks per item and microcracked items percent for butterflies

To date, the most promising alloys are the red gold refined with size 2 ruthenium nanoparticles (alloy L) and size 3 ruthenium nanoparticles (alloy M), therefore not with the smallest particles among those tested (size 4, alloy N). Specifically (Figure 29), alloy L exhibits the lowest percentage of cracked and microcracked items (over 80% reduction compared to alloy C), whereas alloy M achieves the minimum number of cracks and microcracks per individual item (nearly 70% reduction). Additional statistical trials are required to confirm and further validate these findings with greater accuracy.

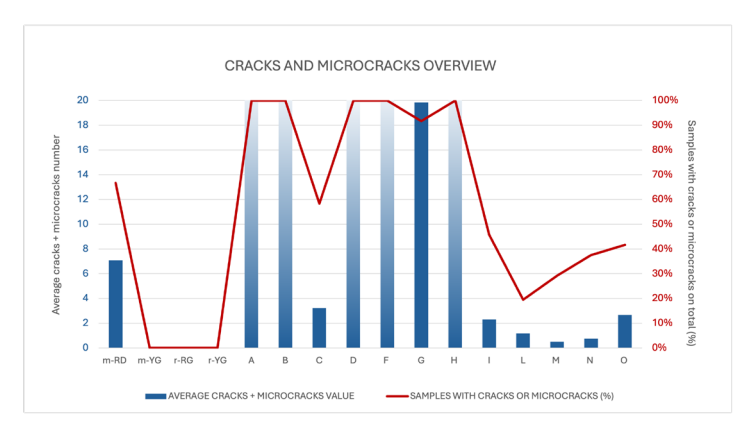


Figure 29: Average cracks and microcracks per item and percentage of cracked or microcracked items

33

Notably alloy (O), where an intermetallic ruthenium compound has been used as refiner, has not provided improvement in grain size and cracks reduction respect to standard alloy (C). This is likely due to the rapid reaction of undissociated intermetallic molecules and atoms with residual oxygen, carbon, and other foreign contaminants, thereby losing much of their effectiveness as refiners.

An additional test was conducted to evaluate the influence of cooling time on the microstructure of the cast items and their resistance to fire cracking. This investigation was driven by the need to understand whether the phenomenon of hot tearing, which is associated with the presence of silicon in the alloy, could potentially affect the alloy's resistance to firecracking. While this effect is significantly less pronounced in red gold compared to yellow gold alloys, it could still lead to the formation of microcracks that may act as initiation sites for fracture propagation during fire cracking tests. Hot tearing is less likely to occur with longer cooling times; however, prolonged cooling can also promote grain growth, potentially compromising resistance to fire cracking. To identify which mechanism is more influential and assess whether cooling time impacts fire cracking resistance, a test was carried out using alloy (C), increasing the flask cooling time from five to ten minutes.

After metallographic etching almost no change in the grain size of the cast items was observed with five- and ten-minutes cooling time (Table 6). An improvement observed with the extended cooling time (10 minutes) was a significantly reduced number of average cracks and a lower percentage of damaged items (Figure 30). This may be attributed to a potential decrease in microcracks caused by hot tearing, which could otherwise serve as initiation sites for fracture propagation during firecracking tests.

ALLODI

Table 6: Grain size of alloy (C) as a function of cooling time

	BRIDGE RINGS		WEDDING RINGS		EARRINGS		BUTTERFLIES		HARD	GRAIN SIZE	
ALLOY	MICRO CRACKS	CRACKS	MICRO CRACKS	CRACKS	MICRO CRACKS	CRACKS	MICRO CRACKS	CRACKS	SPOTS	UP (mm ± s)	DOWN (mm ± s)
C	2.9	1.0	5.0	1.1	1.8	0.3	0.7	0.1	0	955 ±	1405 ±
(5 MINUTES)	89%	33%	89%	44%	22%	11%	33%	11%		387	851
C	5.2	0.8	1.7	0.5	1.3	0.0	0.2	0.0	0	941 ±	1305 ±
(10 MINUTES)	100%	50%	50%	17%	33%	0%	17%	0%		361	641

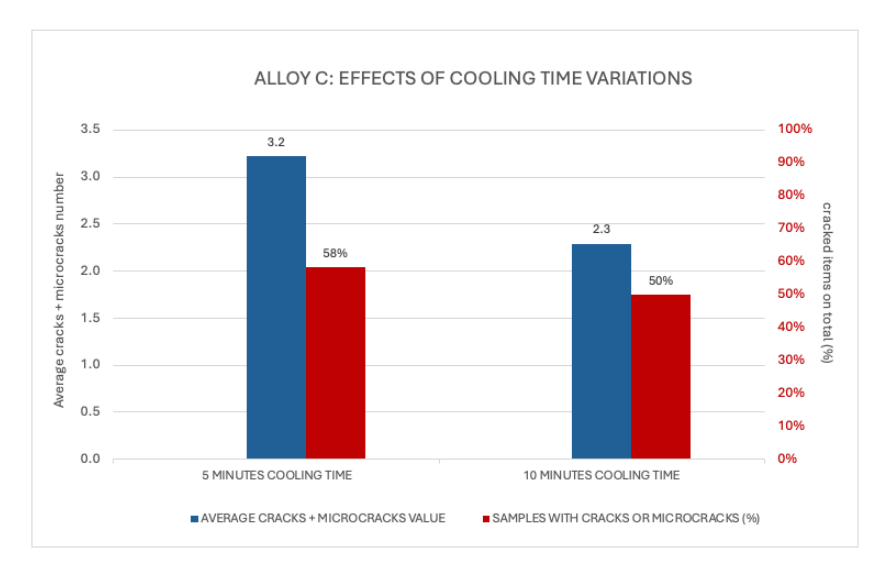


Figure 30: Effects of cooling time variations on firecracking resistance

## **CONCLUSIONS**

The brittleness of commercial 18K red gold alloys has been effectively demonstrated through localized heating of as-cast items using a firecracking test, performed with the torch flame of a water soldering machine designed for goldsmithing. The sensitivity of these alloys to firecracking was found to be primarily due to lattice ordering phenomena in copper-rich materials, specifically order-disorder transitions. These structural transformations result in a significant increase in hardness (from about 170 HV to 300 HV) and an increase in bulk density (e.g., 2–3%), which together induce substantial mechanical stress and a pronounced increase in material fragility.

The study confirms that the fire cracking phenomenon can be successfully mitigated by the incorporation of grain-refining elements such as iridium and ruthenium. However, to enhance the quality of these alloys—particularly in applications like stone-in-place investment casting and filigree parts—the inclusion of deoxidizing elements like silicon is necessary to achieve high surface shininess and cleanliness. The potential interaction between these components, which can reduce the effectiveness of the refiner and, in severe cases, form hard spots visible after the finishing process, presents a critical challenge.

This research explored various methods to enhance grain refinement in deoxidized 18K red gold alloys, focusing on improving resistance to fire cracking. Among the techniques analyzed, the use of nanometric ruthenium powders proved to be the most effective. Alloys refined with this method demonstrated a significant improvement in firecracking resistance compared to both iridium-refined alloys, which exhibited a 100% failure rate due to firecracking, and alloy refined with the standard ruthenium-based process currently employed by Progold.

Notably, the nanometric ruthenium approach led to a reduction of over 80% in the average number of cracks per piece and nearly 70% in the number of pieces exhibiting cracks compared to standard ruthenium-based alloy. These improvements can be attributed to the superior grain refinement achieved with the use of ruthenium nanoparticles, which increased the resistance to the structural stresses associated with order-disorder transitions in copper-rich alloys. These findings highlight the critical role of advanced refining techniques in reducing firecracking and improving the mechanical reliability of red gold alloys.

Future research will focus on optimizing the use of nanometric ruthenium powders and investigating other innovative refiners to further enhance firecracking resistance. For example, further studies will examine the effects of other refiners tested in this work at concentrations different from those analyzed thus far. Additionally, optimizing the amount of silicon used in the alloy could lead to further improvements in firecracking resistance without compromising the alloy's deoxidation efficiency and surface luster. Finally, optimizing the waiting time before cooling the casting flask may represent another key step toward minimizing firecracking, paving the way for more durable and high-performing red gold alloys.

#### **REFERENCES**

- Christopher Corti, "Basic Metallurgy Of Precious Metals, Part II: Cracks And Defects, Their Causes And Prevention," The Santa Fe Symposium on Jewellery Manufacturing Technology, ed. Eddie Bell (Albuquerque: Met-Chem Research, 2019).
- 2. Patrizio Sbornicchia et al., "Understanding Gold Alloy Features from Thermodynamics Phenomena", *The Santa Fe Symposium on Jewellery Manufacturing Technology*, ed. Eddie Bell (Albuquerque: Met-Chem Research, 2018).
- 3. Richard Hertzberg, Deformation and Fracture Mechanics of

- Engineering Materials (John Wiley & Sons, 1983).
- 4. Robert Errichello et al., "Influence of Grain Size on Metallurgical Properties" Gear Technology, (2023).
- 5. A. Pineau et al., «Overview article, Failure of Metals I Brittle and Ductile Fracture,» Acta Materia 107, (2016).
- 6. G.M. Ingo et al., "Thermochemical and Microstructural study of modified CaSO<sub>4</sub> bonded investment with inorganic and organic additives", The Santa Fe Symposium on Jewellery Manufacturing Technology, ed. Eddie Bell (Albuquerque: Met-Chem Research, 2001).
- G.M. Ingo et al., "CaSO<sub>4</sub> bonded investment for casting of gold-based alloys: Study of the thermal decomposition", The Santa Fe Symposium on Jewellery Manufacturing Technology, ed. Eddie Bell (Albuquerque: Met-Chem Research, 1999).
- 8. Dieter Ott, "Reactions of molten metal with investment", The Santa Fe Symposium on Jewellery Manufacturing Technology, ed. Eddie Bell (Albuquerque: Met-Chem Research, 1990)
- 9. Daniele Maggian et al., "The role of silicon in Investment Casting, A case study of the Reactivity of Various Metals with the Investment," *The Santa Fe Symposium on Jewellery Manufacturing Technology*, ed. Eddie Bell (Albuquerque: Met-Chem Research, 2005).
- Greg Normandeau, "The Optimisation of Silicon Alloying Addition in Carat Gold Casting Alloys", Gold Technology (1995).
- 11. Dieter Ott, "Optimising Gold Alloys for Manufacturing", Gold Technology 34 (2002).
- 12. Yunping Ji et al., "Roles of Lanthanum and Cerium in Grain Refinement of Steels during Solidification", Metals 8 (2018): 884
- 13. Qiang Zeng and Shilang Xu, "Thermodynamics and Characteristics of Heterogeneous Nucleation on Fractal Surfaces", The Journal of Physical Chemistry C 119 (2015).
- 14. Farid Abraham, Homogeneous nucleation theory, (Academic Press, 1974).
- 15. D. W. Oxtoby, "Homogeneous nucleation: Theory and Experiment" Journal of Physics: Condensed Matter 38 (1992): 4.